Differential cross sections for rotational excitation of NH_3 by collisions with Ar and He: Close coupling results and comparison with experiment

G. C. M. van der Sanden, P. E. S. Wormer, and A. van der Avoird
Institute of Theoretical Chemistry, NSR-Center, University of Nijmegen, Toernooiveld, 6525 ED Nijmegen, The Netherlands

(Received 5 March 1996; accepted 30 April 1996)

By means of the close coupling method we have calculated state-to-state differential and integral cross sections for rotational excitation and inversion of NH_3 by collisions with Ar and He. For NH_3–Ar we used an empirical and a scaled *ab initio* potential, for NH_3–He an *ab initio* potential. The differential cross sections for NH_3–Ar obtained from the empirical potential have an angular dependence that is in closer agreement with experiment than those obtained from the scaled *ab initio* potential. The integral cross sections are reproduced equally well by the two potentials. Also for NH_3–He the differential cross sections are in accordance with experiment. For the integral cross sections the agreement is good too, except for the very small cross sections to some of the higher rotationally excited states. For both complexes the differential cross sections show a strong dependence on energy, both in their angular dependence and in their relative magnitudes. © *1996 American Institute of Physics.* [S0021-9606(96)00630-7]

I. INTRODUCTION

Differential cross sections (DCSs) and integral cross sections (ICSs) for rotationally inelastic scattering are both very sensitive probes of the anisotropy of the intermolecular potential surface. The quality of potential surfaces can therefore be tested by comparing the calculated state-to-state cross sections with experimentally determined ICSs or DCSs. The information that can be derived from DCSs, however, is more detailed than that contained in ICSs, because DCSs yield information about the dependence of the collision dynamics on the impact parameter. Small angle scattering results from collisions with a large impact parameter, and is dominated by the attractive long range part of the potential, whereas large angle scattering originates from collisions with a small impact parameter, that mainly probe the repulsive short range part of the potential. For ICSs it is not possible to relate their magnitude to specific regions of the potential.

In three previous papers we calculated ICSs using the close coupling (CC) method for NH_3–Ar[1,2] and NH_3–He[3] at a relative kinetic energy of 485 and 436 cm^{-1}, respectively, and compared them with experiment. For NH_3–Ar we have used three different potentials, an *ab initio* potential,[4] a potential in which one parameter in the *ab initio* potential was scaled to improve the agreement between bound states calculations and spectroscopic data,[5] and an empirical potential.[6] We found that the scaling of the *ab initio* potential improved the agreement with the experimental scattering data compared to the original *ab initio* potential, just as it did for the bound state spectrum. Best agreement, however, was obtained when we used the empirical potential. For NH_3–He we made use of only one *ab initio* potential, which gave reasonable agreement with the experimental data.[3]

As a further test of our potentials, we present in this paper DCSs obtained from CC calculations and we compare them with experimental DCSs that have recently become available for NH_3–Ar[7] and for NH_3–He[8] at a relative kinetic energy of 1274 and 1130 cm^{-1}, respectively. The calculations were performed at the energies attained in these experiments for both collision complexes, and for the cross sections that are experimentally observed. In the ortho NH_3–Ar calculations we used the two best potentials, i.e., the scaled *ab initio* potential and the empirical potential. For para NH_3–Ar we only used the empirical potential.

To get an idea of the energy dependence of the DCSs, we have also calculated the DCSs for both complexes at the lower energies at which the calculations in our previous papers were performed. The calculations automatically yield ICSs, too. Since the ICSs have also been experimentally determined for the high energies,[8,9] we also compare the theoretical and experimental ICSs at the high energies for both complexes.

The paper is organized as follows: In Sec. II we describe the intermolecular potentials. In Sec. III we outline the settings of the parameters used in the scattering calculations. The results are presented and discussed in Sec. IV and summarized in Sec. V.

II. INTERMOLECULAR POTENTIALS

The empirical and scaled *ab initio* potential surfaces that we used in our NH_3–Ar calculations are described in Refs. 6 and 4, respectively. The *ab initio* potential for NH_3–He is described in Ref. 3. Here, we summarize the most important features of the three potentials.

The empirical NH_3–Ar potential surface has been determined from a least squares fit to 61 far infrared and microwave vibration–rotation–tunneling measurements and to temperature dependent second virial coefficients. A surface with 13 variable parameters has been optimized to accurately reproduce the spectroscopic observables, using the collocation method for the bound state calculations.[10] This model surface contains long-range attractive forces of induction and dispersion and short range coulombic and electron exchange

repulsive forces. The long-range dispersion coefficients were taken from *ab initio* calculations,[4,11] since they cannot be properly derived from experiment. The three intermolecular coordinates (R,ϑ,φ) were treated without invoking any approximation regarding their separability.

The NH_3–Ar *ab initio* potential has been obtained from Heitler–London short range calculations and from multipole-expanded dispersion and induction long-range contributions. The *ab initio* potential for NH_3–He has been obtained from supermolecule self-consistent field calculations, supplemented with multipole-expanded dispersion contributions at the time-dependent coupled Hartree–Fock plus second order true correlation level.[11] For both potentials a Tang–Toennies-like damping was applied to the long-range energy. The *ab initio* potentials are expressed with respect to a body fixed coordinate frame in which the z axis coincides with the C_3 axis of ammonia, with the nitrogen atom being on the positive z axis. The frame origin is in the center of mass of NH_3 and one hydrogen nucleus is put into the x–z plane, with positive x. The position vector $\boldsymbol{R}$ of the Ar or He atom is given by its usual spherical polar coordinates (R,Θ,Φ). Both potentials are expanded in spherical harmonics $Y_{\lambda\mu}$ through $\lambda=7$

$$V(R,\Theta,\Phi)=\sum_{\lambda\mu} v_{\lambda\mu}(R)Y_{\lambda\mu}(\Theta,\Phi). \tag{1}$$

Due to the threefold symmetry of the ammonia only terms with $\mu=0,3,6,\ldots$ are present. The scaling of the NH_3–Ar *ab initio* potential consists in multiplying a short range parameter in one of the expansion coefficients, $v_{33}(R)$, by a factor of 1.43. This appeared to improve the agreement with the spectrum considerably.[5]

The empirical potential is expressed in a frame that is slightly different from the one used for the *ab initio* potentials, i.e., the nitrogen atom is put on the negative z axis. This means that we have to apply the transformation $\Theta=\pi-\vartheta$ and $\Phi=\varphi$, in order to express both potentials in the same coordinate system.

In the present calculations the potential surfaces are 3-dimensional, i.e., they do not depend explicitly on the ammonia inversion coordinate. This implies that we have to apply the delta function model[12,13] to treat the NH_3 inversion motion. It has been shown,[1] however, that this has only a small effect—in the order of 3%—on the cross sections as compared to calculations that take the inversion coordinate explicitly into account.

III. COMPUTATIONAL ASPECTS

The close coupling calculations were carried out with the HIBRIDON inelastic scattering code.[14] An explanation of the parameters used in the calculations can be found in Ref. 1.

The values of the total energies $E_{\rm tot}$ in the present calculations are given in Table I. The values of the higher energies, 1274 cm^{-1} for NH_3–Ar and 1130 cm^{-1} for NH_3–He, are determined by the total energies in the experiments[7,8] with which we compare our differential cross sections. The lower energies are set to 485 and 436 cm^{-1} for NH_3–Ar and NH_3–He, respectively. These values are determined by the settings in earlier calculations, in which we compared theoretical ICSs with experimental ones.

TABLE I. The total collision energies $E_{\rm tot}$, the maximum symmetric top quantum numbers $(j_{\rm max},k_{\rm max})$ of the levels in the rotational basis set, the total number of (open and closed) levels and the number of accessible (open) levels included in the rotational basis, the lowest energy $(E_{\rm omitted})$ of the states omitted from this basis, the maximum number of channels $n_{\rm max}$, the maximum overall rotational quantum number of the complex $J_{\rm max}$ and the IBM RS/6000–370 CPU times for HIBRIDON versions 3.8 and 4.0, in the calculations for the NH_3–Ar and NH_3–He collision complexes. Given in parentheses in the column ''open'' is the number of levels with $j>j_{\rm max}$ and an energy less than $E_{\rm tot}$, that is omitted from the rotational basis set.

	$E_{\rm tot}$		Levels		$E_{\rm omitted}$			CPU
Atom	(cm^{-1})	$(j_{\rm max},k_{\rm max})$	Total	Open	(cm^{-1})	$n_{\rm max}$	$J_{\rm max}$	(h)
			ortho NH_3					
Ar	485.0	(9, 9)	34	19(0)	798.9	219	150	24
Ar	1274.0	(12,12)	57	49(0)	1285.6	484	250	160
He	436.0	(9, 9)	34	19(0)	798.9	219	160	2
He	1130.0	(11, 9)	48	43(2)	1027.1	372	100	12
			para NH_3					
Ar	501.2	(9, 8)	66	40(0)	729.8	441	150	286
Ar	1290.2	(12,11)	112	96(0)	1369.2	972	250	1035
He	452.2	(9, 8)	66	34(0)	729.8	441	160	18
He	1146.2	(11,11)	96	86(2)	1110.7	772	100	180

The difference in the ortho and para total energies is caused by the difference in ground state energy of the two species. The ortho NH_3 with initial state $j=k=0$, where j and k are the symmetric top quantum numbers of the NH_3 monomer, has zero internal energy, so the total energy is equal to the relative kinetic energy. The initial $j=k=1$ state of para NH_3, which is the ground state of this species, has an internal energy of 16.245 cm^{-1}.[15] The total energy for para NH_3 is consequently set 16.245 cm^{-1} higher than the total energy for ortho NH_3.

For the reduced masses of NH_3–Ar and NH_3–He we have used the values 11.9396 and 3.2408 amu, respectively. The values for the rotational constants of NH_3 are taken from Ref. 15: $B=9.9402$ cm^{-1} and $C=6.3044$ cm^{-1}.

Table I also lists the maximum values of j and k in the rotational basis set, the total number of levels and the number of accessible levels included in the calculations, the lowest energy $(E_{\rm omitted})$ of the states omitted from the rotational basis, the maximum number of channels, the maximum overall rotational quantum number J of the complexes, and CPU times rounded to the hour. The number of open levels omitted from the rotational basis set—because of the limitation on j—is also given in parentheses in the column ''open.'' The difference between $E_{\rm tot}$ and $E_{\rm omitted}$ is a measure for the convergence with respect to the size of the rotational basis. For He in the higher energy case $E_{\rm omitted}$ is slightly smaller than $E_{\rm tot}$. However, it must be realized that the energy of an NH_3 rotational level (j,k) is given by $E_{jk}=Bj(j+1)+(C-B)k^2$, i.e., that E_{jk} decreases with increasing $|k|$, and that the highest included rotational energy level in this case is 1312.1 cm^{-1} for ortho $(j=11,k=0)$ and

1308.5 cm^{-1} for para NH_3 ($j=11,k=1$), so that we do include some states with an energy larger than E_{omitted}.

For He–NH_3 at 1130 cm^{-1}, it proved to be sufficient to retain all levels in the rotational basis set up to $j=11$; going from $j_{\max}=10$ to $j_{\max}=11$ changed the cross sections by less than 1%. For Ar–NH_3 at 1274 cm^{-1}, we had to include all levels up to $j=12$, since going from $j_{\max}=11$ to $j_{\max}=12$ still introduced changes in the cross sections of about 10%. We could not perform calculations at $j_{\max}=13$ since the maximum value of j in the program is 12. However, we estimate the difference between the results obtained with $j_{\max}=12$ and $j_{\max}=13$ to be smaller than 5%. In the lower energy case, both for Ar–NH_3 and for He–NH_3, the value of $j_{\max}$ was 9. Retaining all levels up to $j=11$ changed the cross sections by less than 3%.

In all calculations J took the values $0,1,2,\ldots,J_{\max}$, with $J_{\max}$ given in Table I, and taken large enough to obtain convergence. It is remarkable to see that in the case of He–NH_3 the value of $J_{\max}$ at which convergence is reached, is higher for the low energy. The opposite is true for Ar–NH_3. The quantum number J can be regarded as the quantum mechanical analog of the classical impact parameter.[7] If the potential would still be nonzero at infinity, all impact parameters would contribute, and the value of $J_{\max}$ would be determined by the value of J at which the overall rotational energy starts to take up all the available energy. So one would expect $J_{\max}$ to increase with increasing energy. However, if the range of the potential is short, only a limited amount of impact parameters will contribute. When the total energy of the collision increases, the distance at which the potential becomes negligible compared to the total energy gets smaller, and the number of significant impact parameters decreases. Apparently, the potential of Ar–NH_3 has such a long range that the second effect does not dominate, whereas it does for He–NH_3.

The error in the cross sections due to the finite step size in the propagator was about 1% in all calculations. The step size for the He calculations at both energies was 10 times larger than that of the Ar calculation at the low energy. At the high energy for Ar, the latter step size was multiplied by 2 to keep the calculations feasible. Although the step size should decrease with increasing energy, the convergence was still within a few percent. We have used the possibility of the program to include only open levels in the rotational basis set when the overall rotation of the complexes starts to take up a large part of the available energy. The values of J at which we start to reduce the size of the rotational basis set is 75, 35, 40, and 20 for the successive energies and complexes that are listed in Table I, for both NH_3 species. The effect of this reduction on the cross sections is found to be about 1% in all cases. The fact that the values of J at which the reduction starts are smaller for the higher energies is caused not only by the smaller difference between E_{tot} and $E_{\max}$, but also by the decrease of the level density with increasing energy.

It is not possible to give precise timings for the calculations at the higher energies, since all of them had to be restarted in the course of their runs. Moreover, the calculations were done with different versions of HIBRIDON and on different machines. We therefore give rather crude timings in Table I. The times given are for an IBM RS/6000 model 370 workstation and for the ESSL version of HIBRIDON, version 3.8 or 4.0.

IV. RESULTS AND DISCUSSION

As explained in Sec. III, the calculations for NH_3–Ar were performed at a relative kinetic energy of 1274 and 485 cm^{-1}. The relative kinetic energies in the NH_3–He calculations were set to 1130 to 436 cm^{-1}. The high energies are equal to the relative kinetic energy attained in the counter-propagating pulsed molecular beam experiments[7–9] to which we compare our results. The lower energies were chosen to correspond to the energies attained in the crossed molecular beam experiments to which we previously compared computed ICSs for NH_3–Ar[16] and NH_3–He.[17] The experiment measures the differences in population of a specific rotation-inversion state $|i\rangle \equiv j_k^{\epsilon}$ before and after the collision. The signal is proportional to

$$\Delta n(i)=\sum_{j\neq i}\left[n(j)\sigma(j\rightarrow i)-n(i)\sigma(i\rightarrow j)\right], \tag{2}$$

where $n(i)$ stands for the initial population of state i, $\Delta n(i)$ is a measure for the collision induced change in that population, and $\sigma(i\rightarrow j)$ is a state-to-state cross section. The population changes $\Delta n(i)$ may become negative. We will nevertheless refer to them as ''cross sections'' (corrected for the imperfect initial state preparation) and we will use the abbreviations ICS and DCS for these population changes as well. In the experiments of Meyer the ortho NH_3 initial state consists of 81% 0_0^+ and 19% 1_0^+ and the para NH_3 initial state of 57% 1_1^+ and 43% 1_1^-, both for NH_3–Ar and for NH_3–He.

In Ref. 3 we found that it is important to take the initial state preparation into account if one wants to make a comparison with experiment, especially for NH_3–He. In order to make the correction for the imperfect initial state preparation, the state-to-state ICSs and DCSs obtained from the calculations must be put into Eq. (2). The contributions from the 1_0^+ state of the ortho species and the 1_1^- state of the para species are taken from the same computations (with the same total energy) as the cross sections from 0_0^+ and 1_1^+. This is justified, because the cross sections are only weakly dependent on energy.

The results of the calculations of the DCSs are displayed in Figs. 1–5. The theoretical cross sections are given in $Å^2$/sr. The angular resolution in the experiment is $\Delta(\cos\Theta)=0.2$ and 0.3 for NH_3–Ar and NH_3–He, respectively. The diffraction oscillations at small angles can therefore not be resolved experimentally. The error in the DCSs is estimated to be $\pm 15\%$. To avoid confusion we remark that if the DCS for a certain final state is dashed in the left panel, it does not necessarily have to be dashed in the right panel; the dashes are only used to get a better distinction between the different DCSs. Since the experiment yields only relative values for the DCSs it was necessary to scale them to enable a com-

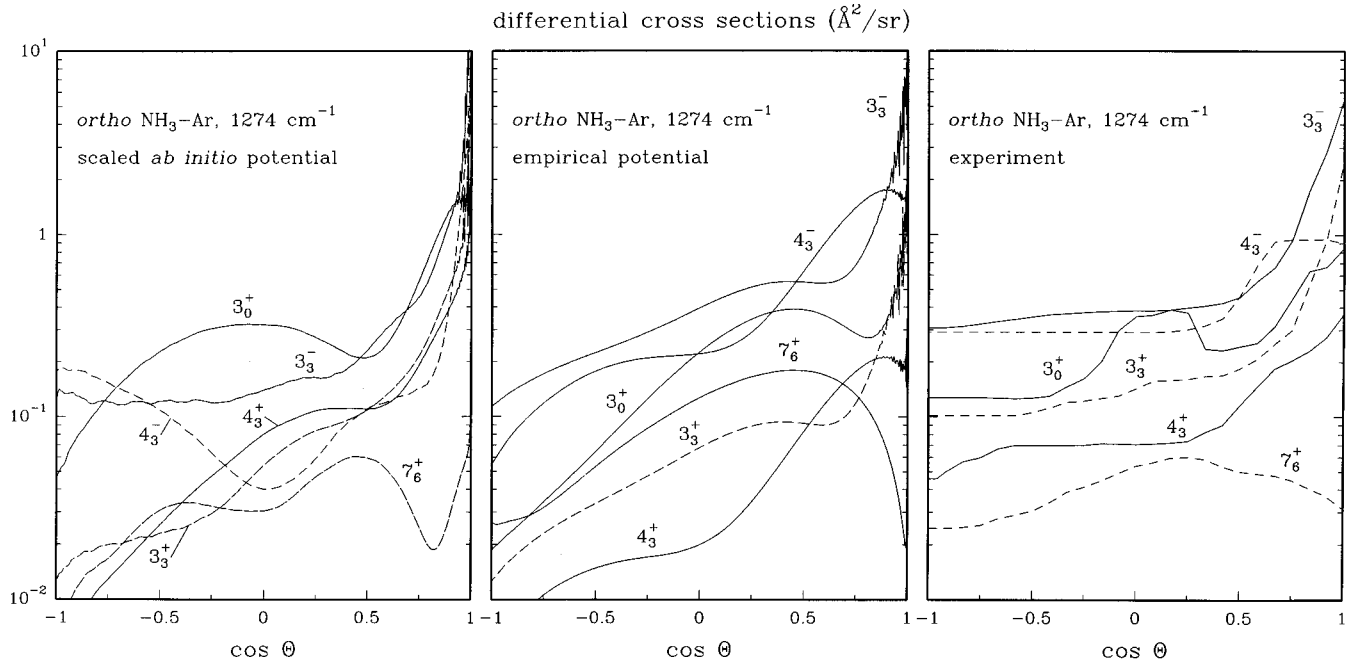

FIG. 1. Theoretical and experimental DCSs for ortho NH_3–Ar at a relative kinetic energy of 1274 cm^{-1}. The theoretical DCSs are calculated from the scaled *ab initio* potential (left) and from the empirical potential (middle). The experimental DCSs (right) are taken from Ref. 7.

parison with the theoretical DCSs. Since it was not possible to find a general recipe for this scaling, we have scaled each case separately, in a way that is described in Secs. IV A and IV B.

In Tables II–VI we have listed both the pure state-to-state ICSs and those that are corrected for the imperfect initial state preparation, together with the experimental ICSs. The theoretical ICSs are given in $Å^2$. As for the DCSs, only relative values for the ICSs can be derived. To facilitate comparison, the sum of the experimental ICSs over all states is set equal to the sum of the corrected ICSs from the present calculations. The sum contains only ICSs for excitations to levels j_k^ϵ that are experimentally observed. The experimental error in the individual ICSs is 10% to 25%. In order to get a single parameter as a measure for the overall agreement between the calculated and experimental ICSs, we have defined an error Q in Ref. 2 in the following way:

$$Q=\left[\frac{\Sigma_i[\Delta n(i)_{\mathrm{calc}}-\Delta n(i)_{\mathrm{exp}}]^2}{\Sigma_i \Delta n(i)_{\mathrm{exp}}^2}\right]^{1/2}\times 100\%, \tag{3}$$

where $\Delta n(i)_{\mathrm{calc}}$ are the corrected calculated ICSs, $\Delta n(i)_{\mathrm{exp}}$ are the experimental ICSs, and the summation runs over all measured final states j_k^ϵ. The values of Q are included in the tables.

A. Differential cross sections for NH_3–Ar

The theoretical and experimental DCSs for NH_3–Ar are shown in Figs. 1–3. In the figures we have indicated the NH_3 species, the relative kinetic energy, and the origin of the DCSs. The experimental DCSs in Fig. 1 are scaled by setting the value of the maximum in the experimental DCS to 3_0^+ equal to the value for that maximum calculated from the empirical potential. In Fig. 2 the experimental DCSs for para NH_3–Ar are scaled by setting the experimental DCS to 4_2 equal to the corresponding theoretical value at $\cos\Theta=-1$.

Figure 1 enables us to compare the DCSs from the scaled *ab initio* potential as well as those from the empirical potential with the experimental ones. The maximum in the experimental DCS to 3_0^+ is reproduced by both potentials. The corresponding angles are $\Theta=80°$, 94°, and 63° for the experiment, the scaled *ab initio* potential, and the empirical potential, respectively.

A somewhat more approximate scattering method is the coupled states (CS) approach. In this approach more symmetry is present than in the CC method, due to the neglect of off-diagonal Coriolis interaction in CS. Thus, CS has certain selection rules that are absent in CC. In the experiment the CS allowed DCSs (with $\epsilon=(-1)^k$) to the states 3_3^- and 4_3^- show an angular dependence that is similar to the angular dependence of their CS forbidden counterparts (with $\epsilon=(-1)^{k+1}$) to 3_3^+ and 4_3^+. This is also the case for the corresponding DCSs obtained from the empirical potential. For the scaled *ab initio* potential, however, the angular dependence of the CS allowed DCSs shows strong deviations from those that are CS forbidden, even at intermediate angles. A characteristic of the experimental CS forbidden DCSs is that they show a stronger decrease towards $\cos\Theta=-1$ than the CS allowed DCSs. This characteristic is exhibited by both potentials (for the $4_3^\pm$ states of the empirical potential, see also Fig. 3). As explained by Meyer,[7] this is related to the fact that the CS approximation becomes better for small impact parameters. As in the experiment, maxima occur in the DCSs to 4_3^- and 7_6^+ for the empirical potential, whereas the scaled *ab initio* potential only gives a maximum

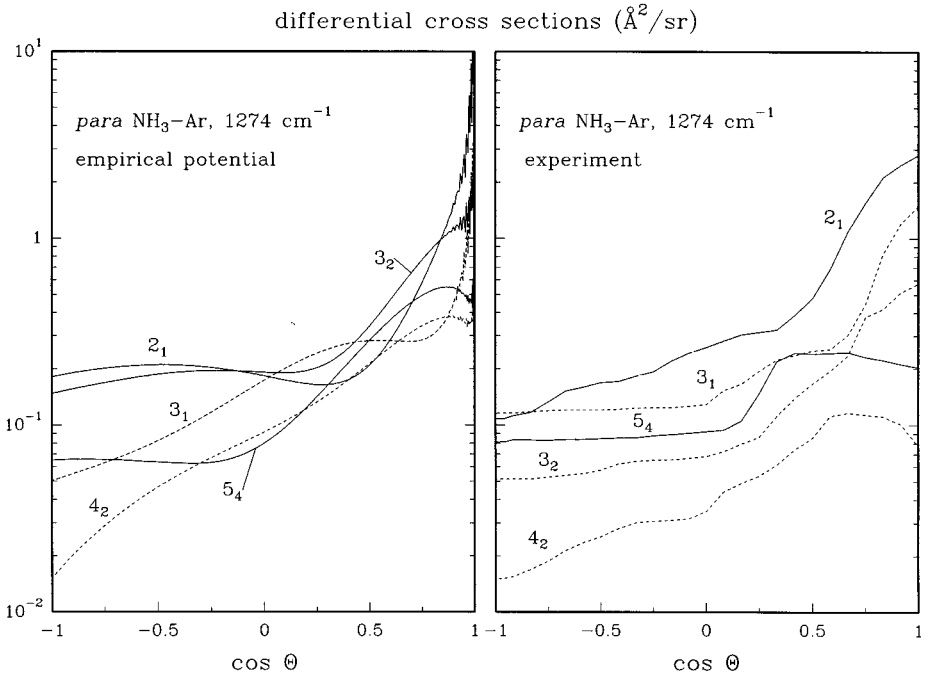

FIG. 2. Theoretical and experimental DCSs for para NH_3–Ar at a relative kinetic energy of 1274 cm^{-1}. The theoretical DCSs (left) are calculated from the empirical potential. The experimental DCSs (right) are taken from Ref. 7.

for 7_6^+. The empirical potential also gives a maximum in the DCS to 4_3^+, contrary to the experiment and the scaled *ab initio* potential.

A remarkable difference between the theory and the experiment is that nearly all computed DCSs continue to decrease exponentially in the backward direction, whereas the experimental DCSs are much more constant in that region. This difference might be caused by the method that is used to derive the angular dependence from the experiment. This dependence is not measured directly, but is obtained via a deconvolution procedure that introduces uncertainties in the experimental Θ dependence.

In view of the findings above and the cost of the calculations we have chosen to restrict our attention to the empirical potential. In the para calculation at 1274 cm^{-1}, and in the calculations at a relative kinetic energy of 485 cm^{-1} only the empirical potential was used.

The DCSs for para NH_3–Ar are displayed in Fig. 2. The largest discrepancy between the theoretical and the experimental DCSs is in the relative magnitude of the DCS to 3_2. However, many of the features of the experimental DCSs are exhibited by the theoretical ones. The experimental DCSs to 2_1, 3_1, and 3_2 have maxima in the forward direction, in the backward direction they are nearly constant. The corresponding theoretical DCSs have the same characteristics, except that the computed DCS to 3_1 continues to decrease at large angles. Both in the theory and in the experiment we can distinguish a shoulder in the DCS to 3_1. The maxima in the DCSs to 4_2 and 5_4 are also reproduced by the theory, even though the angles at which they occur are somewhat larger. In the backward direction the DCS to 4_2 continues to decrease exponentially, the DCS to 5_4 is practically constant, in the computations as well as in the experiment.

Figure 3 demonstrates that both the angular dependence and the relative magnitudes of the DCSs depend strongly on the energy. The variation in the DCSs as a function of Θ is much smaller if the energy is lower, especially at intermediate angles. The maxima and the shoulders in the DCSs have nearly all disappeared at 485 cm^{-1}.

B. Differential cross sections for NH_3–He

The results of the calculations of the DCSs for NH_3–He are displayed in Figs. 4 and 5. The NH_3 nuclear spin species and the relative kinetic energy are also indicated in the figures. The experimental DCSs for ortho NH_3–He in Fig. 4 are scaled by setting the value of the experimental DCS to 3_3^- at $\cos\Theta = 1$ equal to its theoretical value, for para NH_3–He we set the experimental DCS to 5_4 at $\cos\Theta = -1$ equal to the corresponding theoretical value.

Figure 4 shows the results at a relative kinetic energy of 1130 cm^{-1}, together with the experimentally determined DCSs from Ref. 8. If we look at the DCSs for ortho NH_3–He we see that there is a good qualitative agreement between theory and experiment. The DCS to 3_3^- is dominant at small angles, whereas the DCS to 4_3^- is dominant at large angles. The 7_6^+ DCS for backward scattering is larger than those for 2_0^+ and 3_3^-. Both in theory and in experiment the DCSs to 4_3^- and 5_3^- have a maximum at intermediate angles. The threshold behavior of the DCSs to 7_3^- and 7_6^+ is also reproduced fairly well. In general, the relative magnitudes of the DCSs are in reasonable agreement. The largest deviation occurs for the cross section to 4_0^+. The shoulders in the DCSs to 3_0^+ and 3_3^- are, however, not reproduced by the

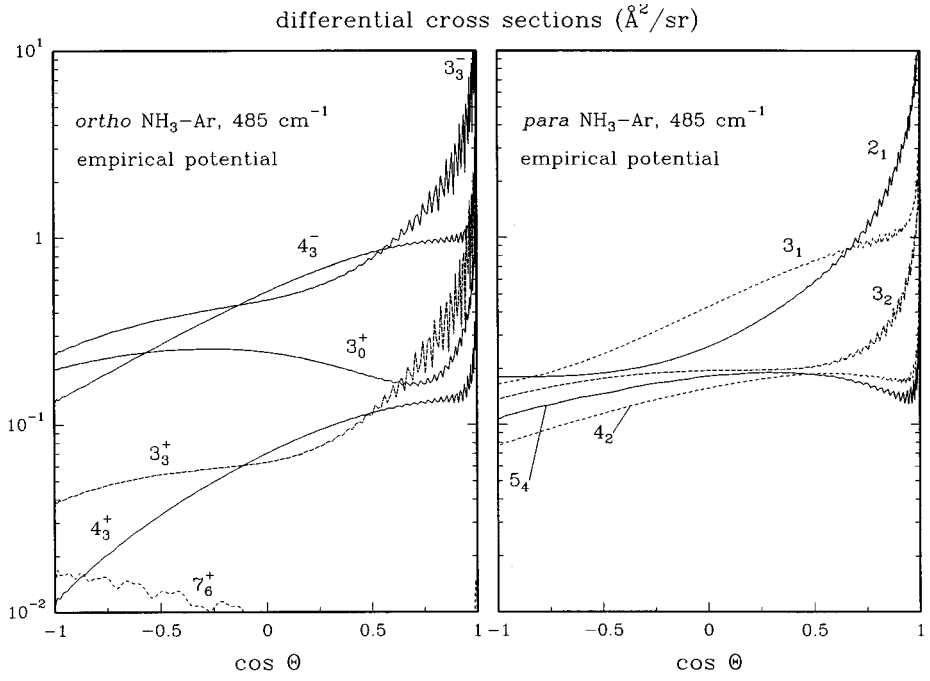

FIG. 3. Theoretical DCSs for ortho NH_3–Ar (left) and para NH_3–Ar (right) at a relative kinetic energy of 485 cm^{-1}. The DCSs are calculated from the empirical potential.

calculations, whereas the shoulder in the DCS to 6_3^- is greatly exaggerated.

We have also compared the angular dependence of the CS allowed and the CS forbidden DCSs. As in the experiment we found that they were very similar over the whole range, and that the CS forbidden DCSs were considerably smaller, to the same extent as in the experiment.

In his discussion of the experimental para NH_3–He DCSs Meyer distinguishes three categories of DCSs.[8] First, DCSs for transitions involving small energy transfer (2_1, 3_1) that are characterized by a maximum at cos $\Theta = 1$, and an exponential decrease towards larger scattering angles. Second, DCSs to states representing intermediate energy transfer (3_2, 4_2, 5_4) that show a rotational rainbow behavior, i.e., they have a maximum which shifts to larger angles with increasing energy transfer. And finally, DCSs to states corresponding to large energy transfer that show a threshold behavior and a maximum excitation probability for backward scattering.

Looking at the results of our calculations, we see that this division into three categories can be made as well for the theoretical DCSs. However, the relative magnitudes of the DCSs are quite different, especially for the DCSs to 2_1, 6_2, 6_4, and 7_4. Also the shoulders in the cross sections to 2_1 and 3_1 do not appear in the theoretical DCSs. We must therefore conclude that the overall agreement between theory and experiment for para NH_3–He is less good than for ortho NH_3–He.

The DCSs computed at an energy of 436 cm^{-1} are shown in Fig. 5. As for NH_3–Ar the relative magnitudes of the DCSs change, and the variation in the DCSs as a function of Θ is smaller. Obviously, fewer states are accessible at the lower energy. For ortho NH_3–He the DCSs to 4_3^- and 5_3^- have lost their maximum and the inflection points in the DCSs to 3_0^+ and 3_3^- have disappeared. The maxima in the para DCSs have disappeared as well, and the DCSs to 2_1 and 3_1 are practically independent of the scattering angle.

Making an overall comparison of the DCSs of NH_3–Ar and NH_3–He, we see that the NH_3–Ar DCSs are much more peaked in the forward direction than those of NH_3–He. Many of the latter DCSs even show a threshold behavior at small scattering angles, and a maximum in the backward direction. These differences in the DCSs are a direct reflection of the differences in the potentials of the two complexes. For NH_3–Ar the long range attraction is much more important than for NH_3–He. As a consequence, the influence of the NH_3–Ar potential is much stronger at large impact parameters than that of the NH_3–He potential. Hence, the NH_3–He DCSs are dominated by short range collisions.

C. Integral cross sections for NH_3–Ar

In Tables II and III we have listed the ICSs for ortho NH_3–Ar for the scaled *ab initio* and the empirical potential, respectively. The ICSs for para NH_3–Ar, for which we only used the empirical potential, are given in Table IV. In Refs. 1 and 2 we also calculated ICSs both for ortho and para NH_3–Ar, at a relative kinetic energy of 280 and 485 cm^{-1}, and we compared them with experiment.[16] The average error Q was found to be 40% for the scaled *ab initio* potential and 26% for the empirical potential. Here, the errors for ortho NH_3–Ar are practically equal for the two potentials, the scaled *ab initio* potential performs even slightly better. An explanation for this finding may be that at an energy as high

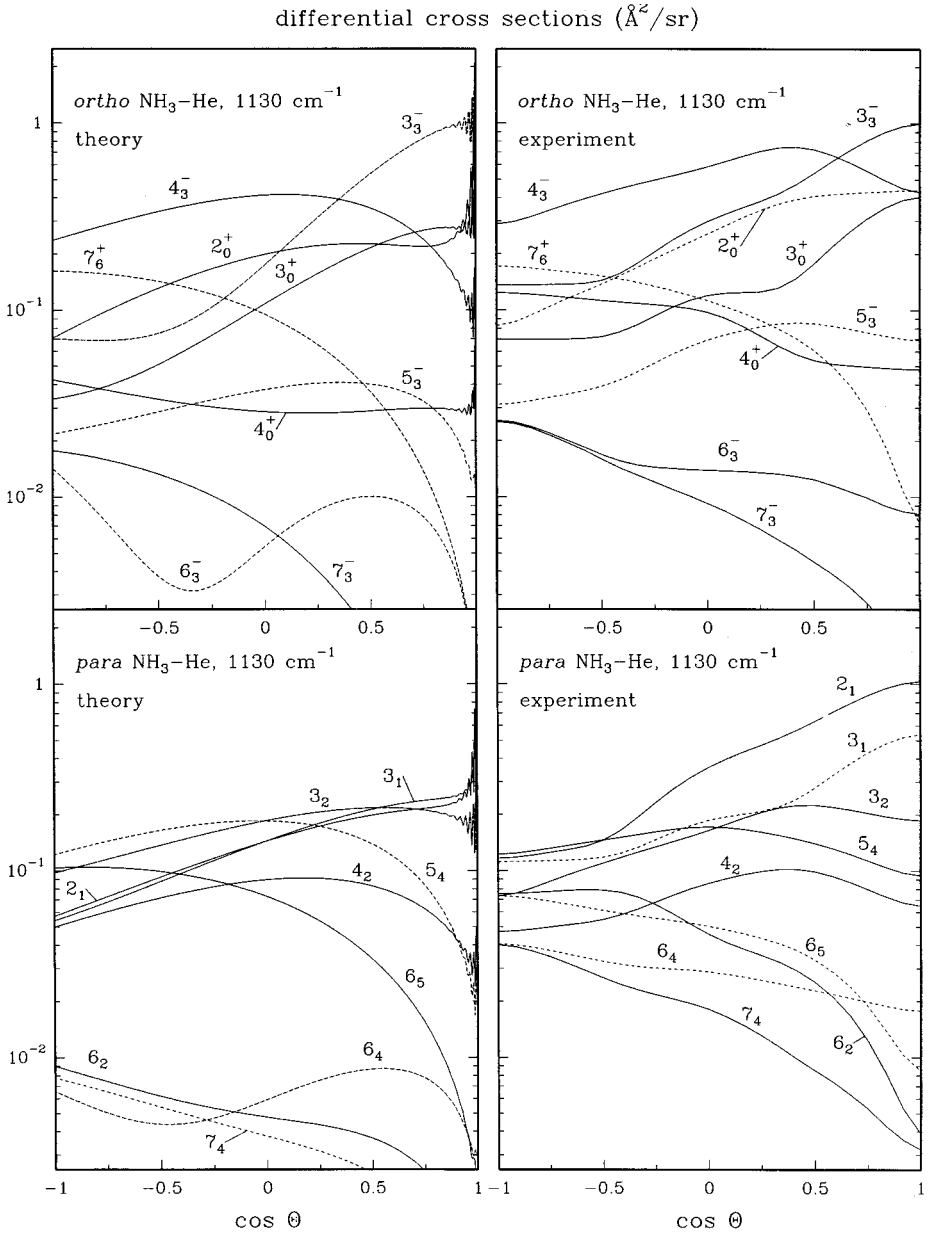

FIG. 4. Theoretical and experimental DCSs for ortho NH_3–He (top) and para NH_3–He (bottom) at a relative kinetic energy of 1130 cm^{-1}. The experimental DCSs (right) are taken from Ref. 8.

as 1274 cm^{-1} the collisions mainly probe the repulsive part of the potential. At lower collision energies the well region of the potential becomes more important. The empirical potential is likely to give a better description of the well region than the scaled *ab initio* potential, since it is determined from the bound state spectrum. The well of the scaled *ab initio* potential, on the other hand, is determined by a delicate balance between the repulsive and attractive contributions to the potential. A small deviation in either of the two contributions already has a large effect on the shape of the well.

If we look at the individual cross sections we see that CS allowed ICSs are clearly larger than the CS forbidden ICSs, in the theory as well as in the experiment, which indicates that the off-diagonal Coriolis interaction is small. The overall agreement with experiment is fairly good for both potentials. The ratio of the corrected calculated cross sections and the experimental ones varies at most by a factor of 2. For ICSs to states with $j>3$ the experimental value is always in between the two theoretical ones. The negative value for the corrected ICS to 1_0^+ indicates that the theory predicts a depletion of this state. Such a depletion has indeed been found in the experiment,[9] although the actual value of this negative cross section has not been experimentally determined.

The results for para NH_3–Ar are given in Table IV. Here the error Q was determined by averaging the calculated corrected cross sections for the two parity states of each rotational level j_k. We note that the experimental values given in Table IV are also the average values of the ICSs to the two inversion states, not their sum.

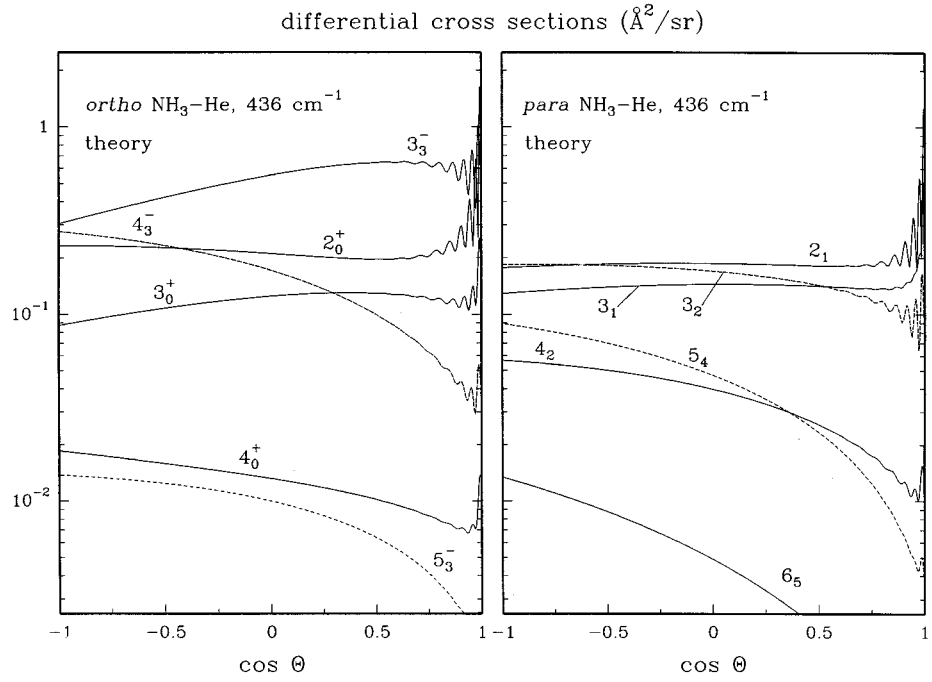

FIG. 5. Theoretical DCSs for ortho NH_3–He (left) and para NH_3–He (right) at a relative kinetic energy of 436 cm^{-1}.

For para NH_3–Ar we find an error of 40%, which is substantially larger than the error for ortho NH_3–Ar. However, if we look at the individual ICSs, again we see that the ratio of the computed and the experimental ICSs varies by a factor of 2 at most, and that the overall agreement between theory and experiment is reasonable.

D. Integral cross sections for NH_3–He

The ICSs for ortho and para NH_3–He are listed in Tables V and VI. As indicated in the tables, the values of the error Q are 23% and 45%, respectively. It is remarkable to see that both for NH_3–Ar and for NH_3–He the error for the ortho species is about 25%, whereas the error for the para species is about 43%. It is difficult to find an explanation for this difference. It is unlikely that the inaccuracies in the potential will have different consequences for the ortho and para species, and our CC calculations are equally well converged for the two species. In our previous study of NH_3–Ar, in which we compared the theoretical ICSs with the experimental results of ter Meulen,[16] the errors for the

TABLE II. State-to-state integral cross sections for ortho NH_3–Ar in Å^2 at a relative kinetic energy of 1274 cm^{-1} using the scaled *ab initio* potential. The calculated cross sections $\Delta n(j_k^\epsilon)$ are corrected for the imperfect experimental initial state preparation as follows [cf. Eq. (2)]: $\Delta n(1_0^+) = 0.81\sigma(0_0^+ \to 1_0^+) - 0.19\Sigma_{i \neq 1_0^+}\sigma(1_0^+ \to i)$, $\Delta n(j_k^\epsilon) = 0.81\sigma(0_0^+ \to j_k^\epsilon) + 0.19\sigma(1_0^+ \to j_k^\epsilon)$, for $j_k^\epsilon \neq 1_0^+$.

		$\Delta n(j_k^\epsilon)$				$\Delta n(j_k^\epsilon)$	
j_k^ϵ	$\sigma(0_0^+ \to j_k^\epsilon)$	Calc	Exp[a]	j_k^ϵ	$\sigma(0_0^+ \to j_k^\epsilon)$	Calc	Exp[a]
1_0^+	5.26	−2.99	–	5_3^+	1.12	0.97	0.4
2_0^+	6.85	6.73	7.2	5_3^-	0.38	0.63	1.4
3_0^+	4.92	4.58	3.1	6_3^-	0.90	0.82	–
4_0^+	0.59	1.07	0.7	6_3^+	0.20	0.28	–
5_0^+	1.00	0.88	0.4	7_3^+	0.17	0.19	–
6_0^+	0.39	0.42	–	7_3^-	0.34	0.33	–
7_0^+	0.12	0.14	–	6_6^-	0.38	0.48	–
3_3^+	0.80	2.29	2.6	6_6^+	0.99	0.97	–
3_3^-	9.14	7.73	6.7	7_6^+	0.46	0.43	0.7
4_3^-	3.25	3.06	5.3	7_6^-	0.06	0.10	–
4_3^+	1.14	1.45	1.3				
Q=26%							

[a]The experimental values from Ref. 9 are multiplied by 1.08.

TABLE III. State-to-state integral cross sections for ortho NH_3–Ar in Å^2 at a relative kinetic energy of 1274 cm^{-1} using the empirical potential. The calculated cross sections $\Delta n(j_k^\epsilon)$ are corrected for the imperfect experimental initial state preparation as indicated in Table II.

		$\Delta n(j_k^\epsilon)$				$\Delta n(j_k^\epsilon)$	
j_k^ϵ	$\sigma(0_0^+ \to j_k^\epsilon)$	Calc	Exp[a]	j_k^ϵ	$\sigma(0_0^+ \to j_k^\epsilon)$	Calc	Exp[a]
1_0^+	7.18	−1.16	–	5_3^+	0.04	0.21	0.4
2_0^+	3.93	4.45	6.7	5_3^-	1.68	1.71	1.3
3_0^+	3.27	2.94	2.9	6_3^-	0.25	0.36	–
4_0^+	0.25	0.58	0.6	6_3^+	0.03	0.04	–
5_0^+	0.53	0.63	0.4	7_3^+	0.01	0.03	–
6_0^+	0.81	0.70	–	7_3^-	0.55	0.46	–
7_0^+	0.04	0.06	–	6_6^-	0.06	0.21	–
3_3^+	0.09	1.35	2.4	6_6^+	0.90	0.85	–
3_3^-	8.73	7.59	6.2	7_6^+	1.44	1.27	0.6
4_3^-	7.37	6.26	4.9	7_6^-	0.02	0.22	–
4_3^+	0.05	0.73	1.2				
Q=29%							

[a]The experimental values from Ref. 9 are multiplied by 1.00.

TABLE IV. State-to-state integral cross sections for para NH_3–Ar in Å^2 at a relative kinetic energy of 1274 cm^{-1} using the empirical potential. The calculated cross sections $\Delta n(j_k^\epsilon)$ are corrected for the imperfect experimental initial state preparation as follows [cf. Eq. (2)]: $\Delta n(j_k^\epsilon) = 0.43\sigma(1_1^- \rightarrow j_k^\epsilon) + 0.57\sigma(1_1^+ \rightarrow j_k^\epsilon)$.

		$\Delta n(j_k^\epsilon)$				$\Delta n(j_k^\epsilon)$	
j_k^ϵ	$\sigma(1_1^- \rightarrow j_k^\epsilon)$	Calc	Exp[a]	j_k^ϵ	$\sigma(1_1^- \rightarrow j_k^\epsilon)$	Calc	Exp[a]
2_1^-	3.69	2.85	3.4	6_2^-	0.08	0.23	–
2_1^+	2.22	3.06		6_2^+	0.33	0.19	
3_1^+	1.88	1.38	0.9	4_4^-	0.94	1.92	1.8
3_1^-	1.00	1.50		4_4^+	2.66	1.68	
4_1^-	1.07	0.56	0.4	5_4^+	2.08	1.04	0.9
4_1^+	0.17	0.68		5_4^-	0.26	1.30	
5_1^+	0.30	0.36	–	6_4^-	0.07	0.39	–
5_1^-	0.41	0.34		6_4^+	0.64	0.31	
6_1^-	0.14	0.35	–	7_4^+	0.04	0.07	–
6_1^+	0.50	0.30		7_4^-	0.09	0.06	
2_2^-	0.02	2.57	4.3	5_5^+	0.05	0.66	0.5
2_2^+	4.49	1.94		5_5^-	1.11	0.51	
3_2^+	3.50	2.04	1.1	6_5^-	1.19	0.56	–
3_2^-	0.95	2.40		6_5^+	0.08	0.71	
4_2^-	1.08	0.85	0.6	7_5^+	0.15	0.40	–
4_2^+	0.68	0.91		7_5^-	0.59	0.34	
5_2^+	0.30	0.28	–	7_7^+	0.11	0.18	–
5_2^-	0.27	0.29		7_7^-	0.23	0.16	

$Q = 40\%$

[a]The experimental values from Ref. 9 are multiplied by 0.73.

TABLE VI. State-to-state integral cross sections for para NH_3–He in Å^2 at a relative kinetic energy of 1130 cm^{-1}. The calculated cross sections $\Delta n(j_k^\epsilon)$ are corrected for the imperfect experimental initial state preparation as indicated in Table IV.

		$\Delta n(j_k^\epsilon)$				$\Delta n(j_k^\epsilon)$	
j_k^ϵ	$\sigma(1_1^- \rightarrow j_k^\epsilon)$	Calc	Exp[a]	j_k^ϵ	$\sigma(1_1^- \rightarrow j_k^\epsilon)$	Calc	Exp[a]
2_1^-	0.53	1.00	1.64	6_2^-	0.02	0.03	0.21
2_1^+	1.36	0.89		6_2^+	0.05	0.03	
3_1^+	0.94	0.97	0.90	4_4^-	0.48	1.52	0.83
3_1^-	0.98	0.96		4_4^+	2.31	1.27	
4_1^-	0.74	0.36	0.30	5_4^+	1.76	0.78	0.64
4_1^+	0.08	0.45		5_4^-	0.04	1.02	
5_1^+	0.51	0.28	0.18	6_4^-	0.02	0.04	0.18
5_1^-	0.10	0.33		6_4^+	0.05	0.04	
6_1^-	0.19	0.14	0.08	7_4^+	0.01	0.03	0.12
6_1^+	0.09	0.15		7_4^-	0.04	0.02	
2_2^-	0.00	1.10	1.64	5_5^+	0.01	0.39	0.22
2_2^+	1.92	0.83		5_5^-	0.67	0.29	
3_2^+	1.54	1.02	0.67	6_5^-	0.74	0.37	0.31
3_2^-	0.62	1.14		6_5^+	0.09	0.46	
4_2^-	0.80	0.41	0.33	7_5^+	0.12	0.08	0.16
4_2^+	0.12	0.51		7_5^-	0.06	0.09	
5_2^+	0.14	0.08	0.17	7_7^+	0.09	0.33	–
5_2^-	0.04	0.10		7_7^-	0.52	0.27	

$Q = 45\%$

[a]The experimental values from Ref. 8 are multiplied by 0.93.

ortho and para species were about the same for the empirical potential. It may be, therefore, that the ICSs from the present experiment are slightly less accurate for the para than for the ortho species.

TABLE V. State-to-state integral cross sections for ortho NH_3–He in Å^2 at a relative kinetic energy of 1130 cm^{-1}. The calculated cross sections $\Delta n(j_k^\epsilon)$ are corrected for the imperfect experimental initial state preparation as indicated in Table II.

		$\Delta n(j_k^\epsilon)$				$\Delta n(j_k^\epsilon)$	
j_k^ϵ	$\sigma(0_0^+ \rightarrow j_k^\epsilon)$	Calc	Exp[a]	j_k^ϵ	$\sigma(0_0^+ \rightarrow j_k^\epsilon)$	Calc	Exp[a]
1_0^+	0.44	−3.03	–	5_3^+	0.01	0.02	0.22
2_0^+	2.62	2.34	1.83	5_3^-	0.17	0.40	0.57
3_0^+	1.72	1.68	1.30	6_3^-	0.07	0.09	0.27
4_0^+	0.16	0.40	0.98	6_3^+	0.01	0.01	0.22
5_0^+	0.96	0.82	0.62	7_3^+	0.00	0.00	–
6_0^+	0.18	0.21	0.23	7_3^-	0.11	0.10	0.21
7_0^+	0.01	0.02	–	6_6^-	0.01	0.24	–
3_3^+	0.01	0.75	0.87	6_6^+	1.31	1.11	–
3_3^-	4.90	4.17	3.20	7_6^+	1.35	1.12	1.33
4_3^-	4.77	4.08	4.20	7_6^-	0.00	0.18	–
4_3^+	0.01	0.44	0.58				

$Q = 23\%$

[a]The experimental values from Ref. 8 are multiplied by 1.21.

If we look at the individual cross sections, we see that the overall agreement is reasonable both for ortho and para NH_3–He. As in the case of NH_3–Ar, the majority of the ICSs differ from the experimental values by less than a factor of 2. There are, however, a few ICSs that show a large discrepancy between theory and experiment. The ICSs to 5_3^+, 6_3^+, 6_2, 6_4, and 7_4 are all practically zero in the theory, whereas they differ significantly from zero in the experiment. A likely cause for the discrepancies is that the quality of the potential is insufficient to accurately predict these small cross sections. We have already seen that our potential is incapable of predicting the rather subtle population changes of states that have both in and out scattering.[3]

We already noted that in scattering calculations for NH_3–He it is very important to take the initial state preparation into account if one wants to make a comparison with experiment. Up to now we only included the first excited state in our correction. In this paper, we have investigated the effect of taking into account the lowest six states in the initial state preparation both for ortho and para NH_3–He, instead of the lowest two. The initial population of these states was taken from Table 2 in Ref. 9. Even though we introduce an error by taking all six initial states from the same computation, i.e., we give them different relative kinetic energies (see also the beginning of this section) we can

get an idea of how important the effect is. The effect is most important on the cross sections to the four states that are now included, in the order of about 10%. The other states are hardly affected. We conclude, therefore, that for the given initial state populations it is not necessary to include more than one excited state.

V. CONCLUSIONS

We have calculated state-to-state DCSs and ICSs for rotational excitation and inversion of NH_3 by collisions with Ar and He using the CC method. In the calculations for ortho NH_3–Ar we have used an empirical and a scaled *ab initio* potential, for para NH_3–Ar we have only used the empirical potential. The NH_3–He calculations were based on an *ab initio* potential. We compare our results to experimentally determined cross sections.

For ortho NH_3–Ar we find that the DCSs obtained from the empirical potential are in closer agreement with the experimental DCSs than those obtained from the scaled *ab initio* potential. For the ICSs, however, the agreement with experiment is about the same for the two potentials. Both for ortho and para NH_3–Ar the empirical potential reproduces the features of the experimentally determined DCSs fairly well, and for both species the ICSs differ by less than a factor of 2 from the experimental ones.

The computed DCSs for ortho NH_3–He are in accordance with the experiment, for the para species some of the relative magnitudes of the calculated DCSs deviate from those in the experiment. Both for ortho and para NH_3–He most of the ICSs differ by less then a factor of 2 from the corresponding experimental ICSs. However, for both species there are a few small ICSs that deviate significantly from their experimental value. It is likely that the discrepancies for NH_3–He are caused by the fact that the potential is not sufficiently accurate.

Both for NH_3–Ar and NH_3–He we find that the angular dependence and the relative magnitudes of the DCSs depend strongly on the energy. A decrease in energy reduces the variation of the DCSs with the scattering angle, especially at intermediate angles. Scattering calculations should therefore be performed at the same energies as the experiment to enable a meaningful comparison.

Finally, we have assessed that it is sufficient to take only the first excited state, which is the dominant contamination, into account when making the correction for the initial state preparation in the experiments to which we compare our results.

ACKNOWLEDGMENTS

We are grateful to Dr. Henning Meyer for making available the figures with the experimental differential cross sections. This work is part of the research program of the ''Stichting voor Fundamenteel Onderzoek der Materie (FOM),'' which is financially supported by the ''Netherlands Organization for Scientific Research (NWO).''

[1] G.C.M. van der Sanden, P.E.S. Wormer, A. van der Avoird, J. Schleipen, and J.J. ter Meulen, J. Chem. Phys. **97**, 6460 (1992); **100**, 5393 (E) (1994).
[2] G.C.M. van der Sanden, P.E.S. Wormer, A. van der Avoird, C.A. Schmuttenmaer, and R.J. Saykally, Chem. Phys. Lett. **226**, 22 (1994).
[3] G.C.M. van der Sanden, P.E.S. Wormer, A. van der Avoird, J. Schleipen, and J.J. ter Meulen, J. Chem. Phys. **103**, 10001 (1995).
[4] M. Bulski, P.E.S. Wormer, and A. van der Avoird, J. Chem. Phys. **94**, 491 (1991).
[5] J.W.I. van Bladel, A. van der Avoird, and P.E.S. Wormer, J. Phys. Chem. **95**, 5414 (1991).
[6] C.A. Schmuttenmaer, R.C. Cohen, and R.J. Saykally, J. Chem. Phys. **101**, 146 (1994).
[7] H. Meyer, J. Chem. Phys. **101**, 6697 (1994).
[8] H. Meyer, J. Phys. Chem. **99**, 1101 (1995).
[9] H. Meyer, J. Chem. Phys. **101**, 6686 (1994).
[10] R.C. Cohen, and R.J. Saykally, J. Chem. Phys. **98**, 6007 (1993).
[11] P.E.S. Wormer and H. Hettema, J. Chem. Phys. **97**, 5592 (1992).
[12] S. Green, J. Chem. Phys. **64**, 3463 (1976).
[13] S.L. Davis and J.E. Boggs, J. Chem. Phys. **69**, 2355 (1978).
[14] HIBRIDON is a package of programs for the time-independent quantum treatment of inelastic collisions and photodissociation written by M.H. Alexander, D.E. Manolopoulos, H.-J. Werner, and B. Follmeg, with contributions by P.F. Vohralik, D. Lemoine, G. Corey, B. Johnson, T. Orlikowski, A. Berning, A. Degli-Esposti, C. Rist, P. Dagdigian, B. Pouilly, and G. van der Sanden.
[15] G. Danby, D.R. Flower, E. Kochanski, L. Kurdi, P. Valiron, and G.H.F. Diercksen, J. Phys. B **19**, 2891 (1986).
[16] J. Schleipen, J.J. ter Meulen, G.C.M. van der Sanden, P.E.S. Wormer, and A. van der Avoird, Chem. Phys. **163**, 161 (1992).
[17] J. Schleipen and J. J. ter Meulen, Chem. Phys. **156**, 479 (1991).